

Nanoscale Resolution with Focused Light: Stimulated Emission Depletion and Other Reversible Saturable Optical Fluorescence Transitions Microscopy Concepts

Stefan W. Hell, Katrin I. Willig, Marcus Dyba, Stefan Jakobs, Lars Kastrop, and Volker Westphal

THE RESOLUTION ISSUE

Although most specifically labeled cellular constituents can readily be detected in a conventional fluorescence light microscope, their submicron-scale structure cannot be perceived. For example, despite the fact that many proteins of the inner mitochondrial membrane can be labeled by tagging with the green fluorescent protein (GFP), the cristae are too small to be represented in an image recorded with light.

Resolution is the minimal distance at which a microscope may discriminate two or more features of the same kind (Abbe, 1873). Therefore, resolution must not be confused with localization precision. While it may easily be possible to localize the center of the fluorescence patch generated by a membrane-labeled synaptic vesicle with nanometer precision in a microscope, its visualization as a 30 to 50 nm hollow sphere fails because the latter requires nanometer scale *resolution*. In fact, conventional epi-fluorescence microscopy may not even resolve two synaptic vesicles touching each other. Similarly, it may be possible to track the trajectory of a single virus particle with nanometer precision but still its inner structure remains elusive to light microscopy.

The resolution limitation is ultimately rooted in the phenomenon of diffraction (Abbe, 1873). Loosely speaking, focusing of light always results in a blurred spot (Born and Wolf, 2002) whose size determines the resolution. According to Abbe, the transverse (i.e., focal plane) full-width at half-maximum (FWHM) of the focal spot is given by

$$\Delta x, \Delta y = \frac{\lambda}{2n \sin \alpha} \quad (1)$$

with λ , n , and α denoting the wavelength, the refractive index, and the semi-aperture angle of the objective lens, respectively. Along the direction of light propagation (i.e., the optic axis), the spot size is about $\Delta z = 2\lambda/(n \sin^2 \alpha)$ (Born and Wolf, 2002).

In the visible optical range, the most sophisticated immersion lenses feature a maximum angle of $\alpha = 73^\circ$; the shortest live cell compatible wavelength is around 400 nm which is almost in the near ultraviolet (UV) (König *et al.*, 1996). Thus, it seemed obvious that if visible light and regular lenses were to be used, the resolution in the focal plane $\Delta x, \Delta y$ would always be poorer than 150 nm (Pohl and Courjon, 1993). In the axial direction the resolution is even worse ($\Delta z > 500$ nm). In recent years significant improvements of axial resolution have been achieved through the coherent use of two opposing lenses as is realized, for example, in 4Pi microscopy (see Chapter 30, *this volume*). However, these systems

are still limited by diffraction. In this chapter, we report on concepts for radically overcoming the diffraction barrier and attaining a resolution of few nanometers: a figure that has been considered impossible with focused light for more than a century.

BREAKING THE DIFFRACTION BARRIER: THE CONCEPT OF REVERSIBLE SATURABLE OPTICAL FLUORESCENCE TRANSITIONS

Since the inception of nonlinear optics (Shen, 1984), it has been speculated that a nonlinear relationship between the applied intensity and the measured (fluorescence) signal could — at least in principle — expand the resolution capabilities of a focusing (far-field) optical system. However, these notions remained vague and without consequence because a concrete physical recipe could not be given. In fact, the multi-photon processes that had initially been considered for significantly improving the spatial resolution turned out to be unsuitable. Therefore, it was not until the early 1990s that concrete physical concepts appeared for breaking the diffraction resolution barrier with focused light (Hell and Wichmann, 1994; Hell and Kroug, 1995; Hell, 1997). In fact these concepts can be viewed as a family of concepts that utilize *reversible saturable optical (fluorescence) transitions*, which we now name reversible saturable optical fluorescence transitions (RESOLFT). They can be described in a common formalism (Hell, 2003).

Let us assume a fluorescent molecule with two distinct states A and B , whereby the transition from $A \rightarrow B$ can be optically induced at a rate $k_{AB} = \sigma I$ [Fig. 31.1(A)]. The variables σ and I denote the transition cross-section and the light intensity, respectively. The rate for the reverse transition $B \rightarrow A$ is denoted with k_{BA} . It may be driven by light, by a chemical reaction, by heat, or any other means, or simply be spontaneous. The kinetics of the molecular states is described by $dN_A/dt = -dN_B/dt = k_{BA}N_B - k_{AB}N_A$, with $N_{A,B}$ denoting the normalized population probability of each state. After a time period $t \gg (k_{AB} + k_{BA})^{-1}$, the populations have reached a dynamical equilibrium at $N_A^\infty = k_{BA}/(k_{AB} + k_{BA})$. The molecule's probability to be in A or B basically depends on k_{AB} and hence on I . At the saturation intensity $I_{sat} = k_{BA}/\sigma$, we have equal probability $N_A^\infty = 1/2$. Increasing $I \gg I_{sat}$ renders $k_{AB} \gg k_{BA}$, so that the molecule is virtually shifted to B : $N_A^\infty \rightarrow 0$.

Figure 31.1(B) illustrates how this behavior can be exploited for creating arbitrarily sharp regions of state A molecules. The scheme in Figure 31.1(B) is one-dimensional (x), but can be

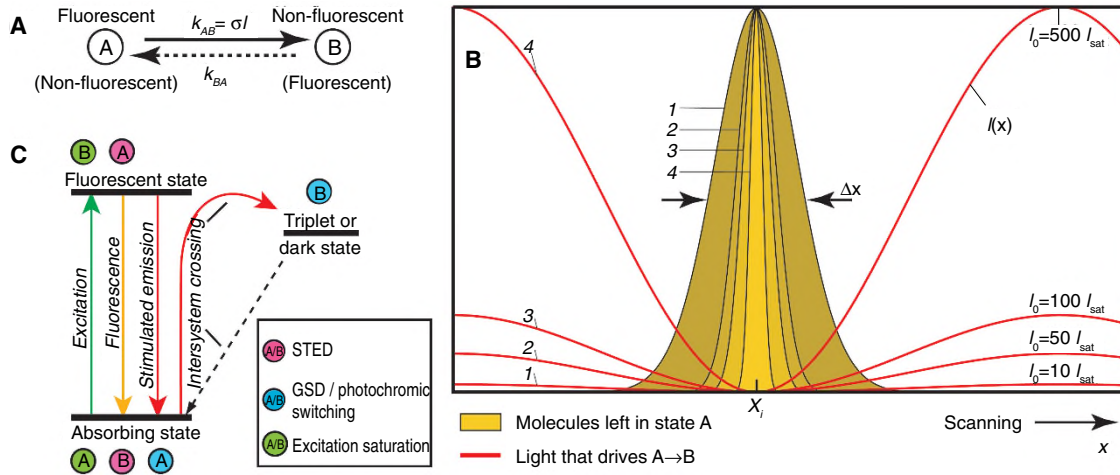


FIGURE 31.1. Breaking the diffraction barrier by reversible saturable optical transitions (RESOLFT) requires (A) two states A and B of a label that are distinct in their optical properties. The optical transition $A \rightarrow B$ takes place at a rate $k_{AB} = \sigma I$ that is proportional to the light intensity I applied. The reverse transition $B \rightarrow A$ of rate k_{BA} brings the label back to its initial state. (B) The profiles 1 to 4 show the spatial region in which the label is allowed to be in state A, if the region is subject to a standing wave of light with peak intensities $I_0 = 10, 50, 100,$ and 500 times I_{sat} and with a zero at x_i . Increasing I_0 ensures that the region in which the label may reside in A is squeezed down, in principle, indefinitely. If A is the fluorescent state of the label, this ultrasharp region functions as the effective fluorescent spot of the microscope and Δx is its FWHM. The creation of a fluorescence image requires scanning that is moving the zero along the x -axis with subsequent storage of the recorded fluorescence. If B is the fluorescent state, then the ultrasharp regions of state A are dark. In this case, a sort of negative image is recorded. Nevertheless, with suitable mathematical postprocessing, similar optical resolution can be obtained. In any case, the resolution is no longer limited by diffraction, but only determined by the value of I_0/I_{sat} . (C) The simplified energy diagram of a fluorophore depicts possible schemes for implementing saturable optical transitions.

readily extended to three dimensions. For this purpose we require the spatial intensity distribution $I = I(x)$ to be zero at a point x_i in space: $I(x_i) = 0$. Whereas in two dimensions or three dimensions, the light intensity distribution would be a two-dimensional (2D) or three-dimensional (3D) doughnut mode, in one dimension the zero is best produced by a standing wave $I(x) = I_0 \cos^2(2\pi n x / \lambda)$. If we now apply $I(x)$ to a spatial distribution of molecules (in x) that are first in state A, then for $I_0 \gg I_{sat}$, virtually all the molecules will be transferred to B, except for those that are very close to x_i . The larger the ratio $I/I_{sat} \gg 1$, the sharper is the region where state A persists [note the increase in curve steepness with increasing saturation level I/I_{sat} in Fig. 31.1(B)]. The FWHM of the resulting spot of state A is readily calculated as:

$$\Delta x \approx \frac{\lambda}{\pi n \sqrt{I/I_{sat}}} \quad (2)$$

In microscopy, the spatial distribution $I(x)$ may be produced by the objective lens itself. If it is produced through the finite aperture of the objective lens, the smallest spot that can be obtained is

$$\Delta x \approx \frac{\lambda}{\pi n \sin \alpha \sqrt{I/I_{sat}}} \quad (3)$$

which may be regarded as an extension of Abbe's equation (Hell, 2003, 2004). In fact, one can easily show that if the zero is produced by focusing the light through the lens, the equation becomes:

$$\Delta x \approx \frac{\lambda}{2\pi n \sin \alpha \sqrt{1 + I/I_{sat}}} \quad (4)$$

For $I/I_{sat} = 100$, the theoretical resolution improvement over Abbe is by about 10. Despite the dependence of Δx on $\lambda/\sin \alpha$ and in contrast to Eq. 1, the new Eqs. 2, 3 and 4 allow diffraction-unlimited spatial resolution.

For a 3D doughnut, we obtain a confined spatial volume of molecules in state A whose dimensions scale inversely with $\sqrt{I_i/I_{sat}}$, $i = x, y, z$, with I_i denoting the peak intensities along the respective axes. Hence, the reduction in volume scales with $\sqrt{I_x I_y I_z / I_{sat}^3}$. In RESOLFT microscopy while the resolution still scales with the wavelength λ , its limit only depends on the applicable light intensity I at a given I_{sat} .

If we now assume that state A but not state B is a fluorescent state, the relevance to imaging becomes obvious: our scheme allows us to create arbitrarily small fluorescence spots (Hell and Wichmann, 1994; Hell, 2003, 2004; Hell *et al.*, 2003). Moreover, by scanning the zero x_i across (or through) the specimen, we can record the fluorophore distribution point by point, and thus assemble a fluorescence 3D image with arbitrary resolution. Identical fluorescent objects can be imaged as separate in space irrespective of their proximity and size because the fluorescence spot (state A) can be made so small that only one of the objects fluoresces.

The concept of RESOLFT inevitably requires scanning (with a zero), but not necessarily with a single beam or a point-like zero. Multiple zeros or dark lines produced by the interference of counter-propagating waves (Cragg and So, 2000; Heintzmann *et al.*, 2002) in conjunction with conventional charge-coupled device (CCD) camera detection can also be used, provided the zeros or the dark lines are farther apart than about the distance required by the diffraction resolution limit of conventional CCD camera imaging (Cragg and So, 2000; Hell, 2003). Dark lines increase the resolution in a single direction only, but stepwise rotation of the pattern plus interleaved scanning of the minima (e.g., by shifting the phase in the interference pattern) and subsequent computational reassignment (Heintzmann and Cremer, 1998; Heintzmann *et al.*, 2002) may provide, under some conditions, similar transverse resolution as with points and do so at higher recording speed. The obligation for scanning remains. The need for scanning is also

the reason why the saturable optical transition $A \rightarrow B$ has to be reversible. The molecule in state B must be able to return to the state A at the latest when the zero comes across its site.

DIFFERENT APPROACHES OF REVERSIBLE SATURABLE OPTICAL FLUORESCENCE TRANSITIONS MICROSCOPY

The RESOLFT scheme and the subsequent breaking of the diffraction barrier is the actual idea behind stimulated emission depletion (STED) microscopy (Hell and Wichmann, 1994; Hell, 1997; Klar *et al.*, 2000). In STED microscopy, many of the molecules that have just been excited to the fluorescent state S_1 (A) are immediately transferred by a further light intensity I to the molecular ground state S_0 (B), so that fluorescence emission is prevented [Fig. 31.1(B,C) and Fig. 31.2(A)]. The physical effect responsible for this transfer is stimulated emission, a basic single-photon phenomenon that has about the same cross-section as single-photon absorption ($\sigma \approx 10^{-16}$ – 10^{-18} cm²). Because STED competes with the spontaneous fluorescence decay of $k_f \approx (1 \text{ ns})^{-1}$ of the S_1 , the saturation intensity I_{sat} can be approximated as k_f/σ or about 10^{25} to 10^{27} photons per square centimeter and second, that is, several tens to a hundred megawatts per square centimeter [Fig. 31.2(B)]. Saturated depletion of the excited state with a focal spot containing a zero squeezes the extent of the fluorescent spot to a subdiffraction size that is not any longer limited by the wavelength,

but only by the applied intensity. The potential and details of STED microscopy will be discussed later.

Other variants of RESOLFT microscopy employing different physical realizations of states A and B have also been suggested [Fig. 31.1(C)] (Hell *et al.*, 2003). For example, in ground state depletion (GSD) microscopy (Hell and Kroug, 1995; Hell, 1997), the ground state S_0 has the role of state A , while state B is a metastable triplet state; more precisely, A and B are the singlet and triplet systems of the dye, respectively. For a number of dyes, intersystem crossing ($A \rightarrow B$) occurs as a byproduct of the regular dye excitation because during each excitation cycle, the molecule crosses to the triplet state with a probability $p \approx 0.05$ to 0.2 . Because of its metastability, the triplet state is relatively easily filled up by repeated regular excitation. For saturation, the triplet buildup rate $k_{AB} = p\sigma I$ must be larger than the decay to the S_0 , $k_{BA} \approx (10^{-6}$ to $10^{-2} \text{ s})^{-1}$, which is comparatively slow. Thus, typical I_{sat} is several tens of kilowatts per square centimeter, which is by 2 to 4 orders of magnitude lower than with STED. Low I_{sat} is invaluable with regard to the attainable resolution (see Eq. 2), and with regard to sample compatibility. However, the experimental realization of this member of the RESOLFT family will be complicated by the fact that the triplet state is involved in the photobleaching pathway (Schäfer, 1973).

Perhaps the simplest way of realizing a saturated optical transition is through an intense excitation (Heintzmann *et al.*, 2002). In this case, the ground state S_0 (A) is depleted and expected to reside in the fluorescent state S_1 (B). The same RESOLFT for-

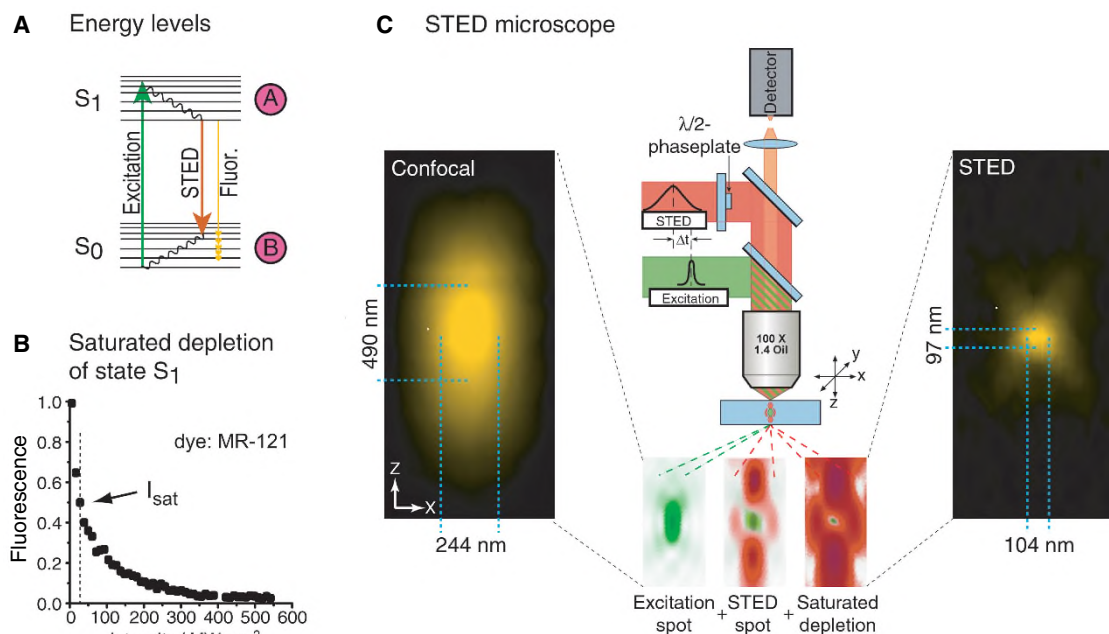


FIGURE 31.2. STED microscopy. (A) Molecules in the fluorescent state S_1 (state A) return to the ground state S_0 (state B) by spontaneous fluorescence emission. Return to S_0 may also be optically enforced through stimulated emission. To prevail over the spontaneous emission, stimulated emission depletion of the S_1 requires relatively intense light pulses with durations of a fraction of the S_1 lifetime. (B) Saturated depletion of the S_1 with increasing peak intensity of STED pulses of ~ 100 ps duration, as measured by the remaining fluorescence of a monomolecular layer of the dye MR-121. For the higher intensity levels, the S_1 is optically depleted. The saturation intensity is defined as the intensity value at which the S_1 is depleted by half. (C) *Center:* Sketch of a point-scanning STED microscope. Excitation and STED are accomplished with synchronized laser pulses focused by a lens into the sample, sketched as green and red beams, respectively. Fluorescence is registered by a detector. *Bottom:* Intensity distributions in the focus. The diffraction-limited excitation spot is overlapped with the doughnut-shaped STED spot featuring a central zero. Saturated depletion by the STED beam confines the region of excited molecules to the zero, leaving a fluorescent spot of subdiffraction dimensions. *Outer left and right insets:* the confocal and the subdiffraction-sized spot left by STED, respectively. Note the doubled lateral and 5-fold improved axial resolution over confocal microscopy. The reduction in dimensions (x, y, z) yields an ultrasmall volume of subdiffraction dimensions, here 0.67 attoliter, corresponding to an 18-fold reduction compared to its confocal counterpart. In spite of using diffraction-limited beams, the concept of STED fluorescence microscopy may, under very favorable conditions, reach spatial resolution at the molecular scale.

malism applies, except that it is state B that is now fluorescent. State A is depleted such that ultrasharp dark regions are created that are surrounded by bright fluorescent regions. In a sense, this approach records negative images, which are subsequently made positive by mathematical postprocessing. The dark regions can be lines produced by interference patterns, but also 3D doughnuts. In the latter case, one would produce dark 3D volumes that are confined by walls of intense fluorescence. The challenges with this otherwise very appealing approach are that the mandatory computations require an excellent signal-to-noise ratio. As with STED, excitation saturation competes with fluorescence emission, so that I_{sat} is also given by k_{fl}/σ which is of the order of 10^{25} photons per cm^2 - second, several tens of megawatts per square centimeter (Hell, 2003). Compared to STED, the intensity needed for saturated optical transitions should actually be up to 10 times lower because the dye can be excited at the maximum of the emission spectrum where cross-sections are largest. Still, intense excitation increases photobleaching. Relief could possibly be brought by using non-blinking semiconductor quantum dots as labels (Alivisatos, 1996; Bruchez *et al.*, 1998; Peng *et al.*, 2000).

Hence, while the family of RESOLFT concepts is not subject to Abbe's diffraction barrier anymore, the dependence of the resolution gain on $\sqrt{I/I_{sat}}$ entails another soft barrier which is the maximum intensity I that the sample can tolerate. Fortunately, the remedy is the use of transitions with low values of I_{sat} , that is, optical transitions that are easy to saturate.

An example is the optical switching of bistable compounds from a fluorescent state (A) into a non-fluorescent state (B), or vice versa. Optical bistability can be realized by photo-induced *cis-trans* isomerization (Dyba and Hell, 2002; Hell *et al.*, 2003). If both states A and B are (meta)stable, the optical transition $A \rightarrow B$ or $B \rightarrow A$ can be completed at very long, if not arbitrary, time scales. Thus, the light energy needed for these transitions can be spread in time (Hell *et al.*, 2003), reducing I_{sat} to values that are lower by many orders of magnitude compared to those of STED or the other RESOLFT family members. These processes would also readily lend themselves for parallelization through large area widefield imaging. However, the principal advantage is the insight that nanoscale resolution does not necessarily require extreme intensities of light (Hell, 2003, 2004; Hell *et al.*, 2003).

Suitable candidates for this concept are the optically switchable fluorescent proteins. For example, the protein asFP595 can be switched on by green light ($B \rightarrow A$) and also switched off ($A \rightarrow B$) by blue light recurrently (Lukyanov *et al.*, 2000; Chudakov *et al.*, 2003). Although known proteins such as asFP595 may have major limitations, such as a low quantum efficiency and a strong tendency to form oligomers, these problems could possibly be solved by strategic mutagenesis. Alternatively, new switchable proteins could be found by targeted exploration. A RESOLFT concept based on genetically encoded optically switchable tags is extremely appealing, because it would allow highly specific imaging in live cells with unprecedented optical resolution. We expect that further variants of RESOLFT will emerge in the future.

STIMULATED EMISSION DEPLETION MICROSCOPY

So far, STED microscopy is the only member of the RESOLFT schemes that has been realized (Klar *et al.*, 2000, 2001). In its initial demonstration, STED microscopy has been realized as a point-scanning system, whereby excitation and STED is performed with two synchronized ultrashort pulses [Fig. 31.2(C)].

The first pulse excites the molecule into the fluorescent state S_1 at a suitable wavelength. The red-shifted second pulse that follows a few picoseconds later transfers the molecules away from the zero back to the ground state S_0 . Although I_{sat} is several tens of megawatts per square centimeter, it scales inversely with the pulse duration of 10 to 300 ps. Because the breaking of the diffraction barrier calls for $I \gg I_{sat}$, focal intensities of 100 to 500 MW/cm² are required (Hell and Wichmann, 1994). For comparison, live-cell multi-photon microscopy typically uses 10^3 to 10^4 times shorter pulses of 10^3 to 10^4 greater intensity: 200 GW/cm². As most sample damage mechanisms depend nonlinearly on the intensity, the typical values used for STED so far have been live-cell compatible (Klar *et al.*, 2000).

Figure 31.2(C) shows a typical experimental focal intensity distribution of the excitation spot (green), overlapping with a STED spot (red) featuring a central hole. Saturated depletion inhibits fluorescence everywhere except for the very center of the focal region (Klar *et al.*, 2000). For the $I/I_{sat} \approx 100$ applied for the measurement in Figure 31.2, the net 3D spot becomes almost spherical with a diameter of ~ 100 nm, which amounts to an almost 6-fold and 2.3-fold increase in axial and lateral resolution, respectively. Although theory permits much higher resolution (in principle, molecular scale), in this experiment the production of a smaller spot was challenged by experimental imperfections (Klar *et al.*, 2000), such as a finite depth of the central zero, and increased photobleaching with increasing I/I_{sat} .

The fact that the spot is squeezed more in the z -direction than in the focal plane is due to the higher local intensity of this particular quenching spot along the optic axis. Using a STED beam of different shape, an improvement of more than 5-fold in the focal plane resolution, compared to Abbe's barrier, has recently been demonstrated with single molecules dispersed on a surface (see Fig. 31.3 and Westphal *et al.*, 2003). Furthermore, Figure 31.3(B) proves that objects separated by much less than the diffraction limit can clearly be distinguished. Recent experiments also indicate that, in accordance with Equations 2 and 3, even higher lateral resolution is possible with STED, provided that photobleaching can be avoided. In fact, it has been shown that a focal spot width of 16 nm, corresponding to little more than 2% of the wavelength used can be obtained [see Fig. 31.7(A)] (Westphal and Hell, 2005). Because the diffraction barrier is broken, STED microscopy does not have a firm resolution limit. The ultimate resolution solely depends on how well the operational conditions can be realized.

In frequency space, the sample structure is described in terms of spatial frequencies. Therefore, microscope performance is defined by the OTF (optical transfer function), describing the strength with which these frequencies are transferred to the image. Thus, the resolution limit is given by the highest frequency that produces a signal above the noise level. Point spread function (PSF) and OTF are intertwined by Fourier mathematics: the sharper the PSF, the broader the OTF. The OTF extension of STED is very smooth [see Fig. 31.3(C)], without any gaps, simplifying the deconvolution techniques needed to produce the best final results.

At present, the fact that relatively few fast, pulsed, tunable, visible lasers are available places some practical limits on the dyes that can be used for STED microscopy. The STED laser system must be able to produce two short laser pulses that follow one another in the picosecond time domain. The first pulse must be at a wavelength capable of exciting the dye, and the second, more powerful pulse must be at a wavelength capable of quenching it. Although early STED studies were confined to red-emitting dyes by the availability of appropriate lasers, this is no longer the case.

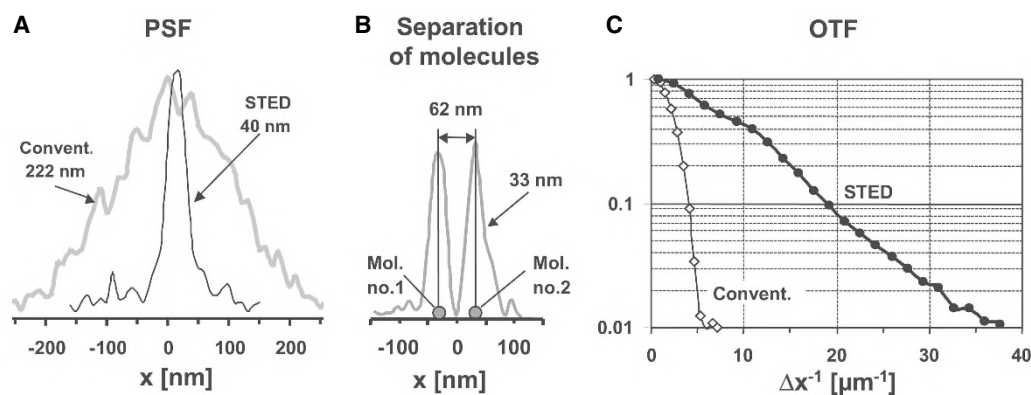


FIGURE 31.3. Quantifying lateral resolution in STED microscopy through imaging of point-like objects. (A) The effective point spread function (PSF) of a conventional microscope and a (laser-diode) STED microscope, determined on single dye molecules (JA 26). (B) Molecules spaced apart far below the diffraction limit could be clearly separated in STED microscopy (slightly augmented by deconvolution). (C) For STED microscopy the gain in transmitted bandwidth of the optical transfer function (OTF) is more than 5-fold, compared with conventional microscopy. Objective lens, NA = 1.4 (oil); wavelengths λ , 635 nm (excitation), 650 to 720 nm (fluorescence detection), 781 nm (STED).

A list of the dyes used so far, is found in Table 31.1. This list is likely to be expanded as the number of pulsed-laser diodes increases and lasers become available that are capable of doing STED on blue, green, and yellow fluorophores, as well as fluorescent proteins. Studies aimed at identifying suitable laser/dye pairs are ongoing.

Recently, a very compact STED microscope was demonstrated using a laser diode for the blue excitation and a second diode laser for STED at around 780 nm (Westphal *et al.*, 2003). As the set of available wavelengths expands over the next decade, it should in the future become possible to realize STED microscopy at lower cost and on most dyes.

Although shorter wavelengths will lead to higher spatial resolution, a further increase in intensity may be barred in aqueous media by intolerable photobleaching. Saturation factors of >200 might not be readily attainable.

STED microscopy is still in its infancy. So far, most of the applications have been aimed at exploring its principles. Tackling cell biology questions will be a task for the years to come. Strong fluorescence suppression (reduction by 90%) is conceptually not mandatory, but practically important to attain subdiffraction resolution. Among the first biological stains described that allows this level of suppression to be reached were lipophilic dyes such as Styryl 6, 7, and 8, 9M, LDS 751, Pyridine 1, 2, 4 and RH 414, or Oxazine 170 and Nile Red. Because STED was first realized with a titanium:sapphire (Ti:Sa) laser emitting in the far-red (750–800 nm), the emission maximum of these dyes is located around 650 to 700 nm (Klar *et al.*, 2000).

Pyridine 4 was used to label the membranes of live *Escherichia coli*. A simultaneous doubling of both the axial and lateral resolution was observed using a 3D doughnut and STED pulses of

~ 30 ps duration. This initial improvement is likely to be augmented by further optimization of the wavelengths, of the doughnut, and of the pulse duration. Indeed, recent studies revealed that STED-related photobleaching dramatically decreases with the duration of the STED pulse, which indicates a strongly nonlinear dependence of bleaching on the STED-pulse intensity (Dyba and Hell, 2003). Although bleaching is substantially reduced with pulses >120 ps duration, more studies are required to address this critical issue.

In budding yeast, the dye RH 414 is taken up by bulk membrane internalization and subsequently transported to the vacuolar membrane. The structural integrity of vacuolar membranes is sensitive to many stress factors. Therefore, the subdiffraction resolution imaging of vacuoles in living yeast by STED microscopy confirmed that STED microscopy is amenable to imaging living cells (Klar *et al.*, 2000).

Recent progress in laser technology has enabled STED microscopy employing dyes that fluoresce in the visible range. These dyes offer several significant advantages: The shorter wavelengths involved inherently improve the Abbe resolution, while a better quantum efficiency [compared with near-infrared (NIR) dyes] leads to brighter images. Furthermore, the fact that they are visible by eye simplifies sample inspection and image region selection. As a first example, a dramatic enhancement of the resolution in the focal plane is demonstrated on yellow-green fluorescent microspheres (FluoSpheres 505/515, Molecular Probes, OR) in Figure 31.4.

Although the principle of STED applies to any fluorophore, new fluorescent markers require prior investigation. Sometimes the narrow spectral window for efficient STED depends on the chemical environment and has to be established through meticu-

TABLE 31.1. Listing of Example Dyes That Have Been Used Successfully for STED

Category	Name	Emission nm	STED nm	Manufacturer	Notes
Green dye*	Atto532	540–570	615	Atto-tec GmbH, Siegen, DE	Used for single-molecule studies
Yellow dye*	DY-510XL	560–630	625	Dyomics GmbH, Jena, DE	Immunofluorescence label
Red dye*	Atto647N	650–720	760	Atto-tec GmbH, Siegen, DE	Used for single-molecule studies
Far red dye	Pyridine 2	680–750	750–780	SigmaAldrich, St. Louis, MO	Membrane label
Infrared dye	Pyridine 4	710–800	780–800	SigmaAldrich, St. Louis, MO	Membrane label

* These dyes have functional groups and can be coupled to proteins making simultaneous, 3-color, immuno-fluorescence STED imaging possible.

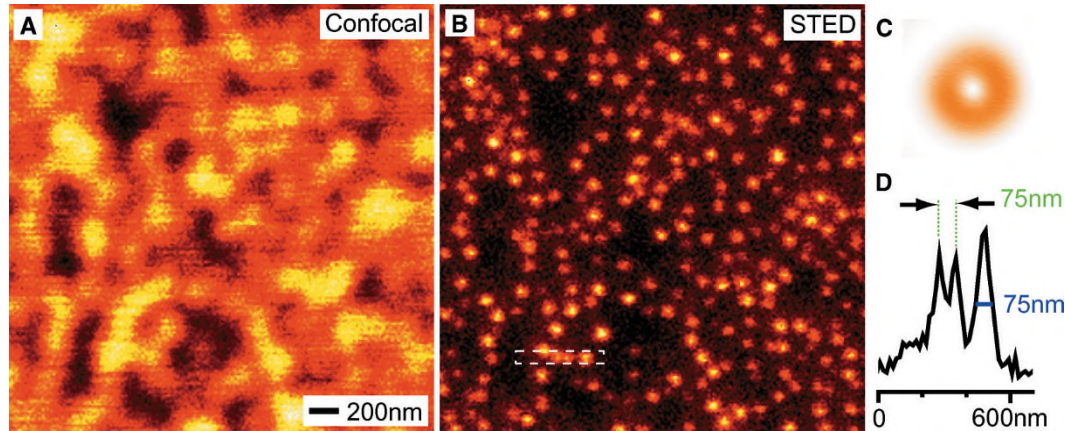


FIGURE 31.4. Beyond the diffraction barrier: STED versus confocal fluorescence microscopy on 40 nm fluorescent microspheres (emission maximum at 515 nm) spread out on a coverslip. The comparison of the confocal (A) and the STED (B) image demonstrates the superior resolution of STED microscopy; neighboring beads are clearly separated. (C) STED intensity distribution employed for depletion, featuring a prominent zero in the center. Drawn to scale with the images. (D) Vertical sum of marked region in (B) illustrates both the clear separation capabilities and subdiffraction resolution of STED microscopy. Objective lens, NA = 1.4 (oil); wavelengths λ , 469 nm (excitation), 500 to 550 nm (fluorescence detection), 585 nm (STED).

lous screening. Ongoing investigations on fluorescent proteins will establish the operational conditions for STED and its potential with these important labels.

Recently, the resolving power of STED has been synergistically combined with that of 4Pi microscopy to achieve nanoscale axial resolution (Dyba and Hell, 2002). Destructive interference of the counterpropagating spherical wavefronts of the STED pulse at

the focal point produces a narrow focal *minimum* for STED with an axial FWHM of $\sim\lambda/(4n) \approx 100$ to 120 nm. Overlap with the regular excitation spot of a single lens has so far rendered focal spots down to $\Delta z = 40$ to 50 nm. Linear deconvolution of the data removes the effect of the weak (<30%) sidelobes that accompany the narrow focal spot. Moreover, it further increases the axial resolution up to 30 to 40 nm. This is exemplified in Figure 31.5(C,D),

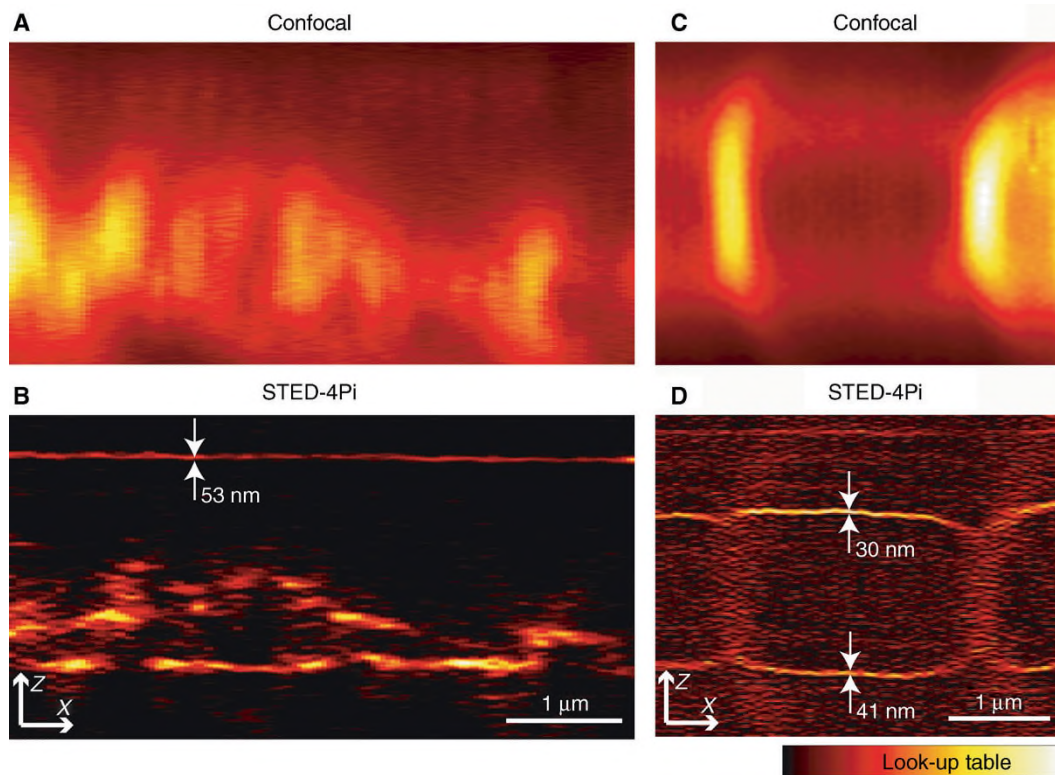


FIGURE 31.5. Axial resolution increase provided by STED-4Pi (B, D) over confocal microscopy (A, C). xz -images from the immunolabeled microtubular network of a HEK cell as recorded with a (A) confocal and (B) STED-4Pi microscope. Both images have been recorded at the same site in the cell. The microtubules were labeled using a primary anti- β -tubulin antibody and a secondary antibody coupled to MR-121. The STED-4Pi images were linearly deconvolved to remove the effect of the 4Pi sidelobes. Note the straight horizontal line which stems from an MR-121 layer on the coverslip. At this layer, the resolution of the STED-4Pi microscope is determined as 53 nm after linear deconvolution. The HEK cell was mounted in aqueous buffer and recorded with water-immersion lenses. In another experiment the membranes of a live bacterium (*Bacillus megaterium*) were stained with the RH 414. Next it was simultaneously imaged in the confocal (C) and in the STED-4Pi microscopy mode (D). Note that the axial resolution of this focusing microscope is of the order of 30 to 40 nm.

which shows xz -images of the membrane-labeled *Bacillus megaterium* (Dyba and Hell, 2002).

The STED-4Pi setup realized so far improves the resolution along the z -axis only, thus rendering a disk-shaped focal spot whose effect is also noticeable in Figure 31.5(B,D). The spot could be sculpted down to a spherical shape by applying a second, STED, pulse whose spatial form is designed to squeeze the spot laterally.

STED-4Pi microscopy has also been applied to the imaging of the microtubular cytoskeleton of human embryonic kidney (HEK) cells (Dyba *et al.*, 2003). The HEK cells were decorated with an anti- β -tubulin antibody and a secondary antibody coupled to the red-emitting dye MR-121. The latter displays high STED efficiency (>90%) at a STED wavelength of \sim 780 to 795 nm. Contrary to the confocal xz -sections, in the linearly deconvolved STED-4Pi counterpart, most of the microtubules appear as distinct objects [Fig. 31.5(A,B)].

The axial resolution attained can be inferred from the FWHM of a fluorescent mono layer that has been deposited on the coverslip; it is \sim 50 nm, corresponding to 1/16 of the irradiation wavelength of 793 nm. It is interesting to note that in the STED-4Pi image, the brightness of the monomolecular layer is of the same order as that of the microtubules. By contrast, in the confocal image, signal from the layer is overwhelmed by the total signal from the larger focal volume of the confocal microscope.

An important task for the near future is to define the optimal parameters for specific imaging applications. The results obtained with STED and STED-4Pi microscopy demonstrate that the basic physical Abbe limit has been broken and we are now moving towards attaining a 3D resolution of the order of a few tens of nanometers.

CHALLENGES AND OUTLOOK

Given the limits on the rate of excitation and fluorescence emission, high temporal and high spatial resolution may be mutually exclusive in many cases, simply because of the poor statistics of the collected photon signal. High spatial resolution also requires small pixels, which is not favorable for fast imaging of large areas. Downsizing the region of interest will be inevitable. A remedy is to parallelize the scanning system, either by applying many foci or by utilizing sophisticated structured illumination schemes. Likewise, the limited number of emission cycles that characterizes many fluorophores, caps the signal that is available from a sample, and, thus, the signal per sample volume. For a number of staining protocols and applications, the available signal might not match up with the number of photons that must be detected in order to benefit from the increase in spatial resolution. Therefore, potential improvements in fluorescent labels as well as strategies for avoiding photobleaching will play a vital role in firmly establishing nanoscale resolution in light microscopy.

Still, even under poor signal conditions, a RESOLFT method creating ultrasmall focal volumes, such as STED, may be extremely helpful for techniques that exploit fluorescence statistics. For example, fluorescence correlation spectroscopy (Magde *et al.*, 1972) depends on small focal volumes to detect rare molecular species or rare molecular interactions in concentrated solutions (Eigen and Rigler, 1994; Levene *et al.*, 2003). STED may be

the key to interrogating nanosized volumes in intact cells. In fact, it is so far the only method reported to squeeze a fluorescence volume to the zeptoliter scale without mechanical confinement. Published results imply the possibility of sampling spherical focal volumes of only 30 nm diameter (Kastrup *et al.*, 2005).

The past decade has witnessed the emergence of a family of physical concepts for attaining diffraction-unlimited spatial resolution in focusing fluorescence microscopy. Relying on reversible saturable optical (fluorescence) transitions (RESOLFT), the spatial resolution of these concepts is eventually determined by the saturation level that can be realized. Saturation brings about an essential nonlinear relationship between the signal and the applied intensity that allows one to overcome diffraction fundamentally.

The nonlinearity brought about by saturation is radically different from that of the well-known multi-photon events. In the latter cases, the nonlinearity stems from the contemporaneous action of more than one photon, which inevitably demands high focal intensities. In contrast, the nonlinearity brought about by saturated depletion stems from the population kinetics of the states involved (Hell, 2003). This opened the door to attaining marked nonlinearities even with linear optical transitions such as single-photon excitation and stimulated emission. Semistable molecular states enable saturable optical transitions at even lower light intensities. Bistable fluorophore constructs and switchable fluorescent proteins should allow very high levels of saturation at the low light intensities essential for live-cell imaging. This insight may be critical to opening up the cellular nanoscale with visible light and regular lenses (Hell, 2003; Hell *et al.*, 2003).

In fact, it is interesting that the demand for high intensities is the reason why the typical nonlinear optical processes of multi-photon fluorescence excitation and multi-photon scattering [second and third harmonic generation (SHG, THG), coherent anti-Stokes Raman scattering (CARS), etc.] could not substantially improve the spatial resolution. It is also clear that as n -photon excitation of the fluorescent state (i.e., the S_1) eventually requires the subdivision of the excitation energy into n photons, it leads to an n times larger wavelength. As an n times larger wavelength leads to n times larger focal spots, multi-photon excitation processes are counterproductive when it comes to sharpening the focal spot size in the focal plane. Exceptions have been given (Hänninen *et al.*, 1996; Schönle and Hell, 1999; Schönle *et al.*, 1999) but they currently appear less promising than the concept of RESOLFT.

The principles of the concept of RESOLFT have been validated through STED microscopy, whose ability to break the diffraction resolution barrier has been experimentally demonstrated. It is worth mentioning that the strategy of utilizing reversible saturable optical transitions also has the potential to break the diffraction barrier in nanoscale writing and data storage (Hell, 2004). The coming years will show whether STED and its RESOLFT cousins are going to establish themselves as part of the microscopic toolbox to elucidate dynamics and structure of cellular networks. The chances are better than ever.

A taste of what is to come can be seen in Figure 31.6, which shows small patches of cell membrane, immuno-stained against the SNARE protein SNAP25, and viewed both by confocal and STED microscopy using the exact same optics. The improvement is even more obvious in Figure 31.7.

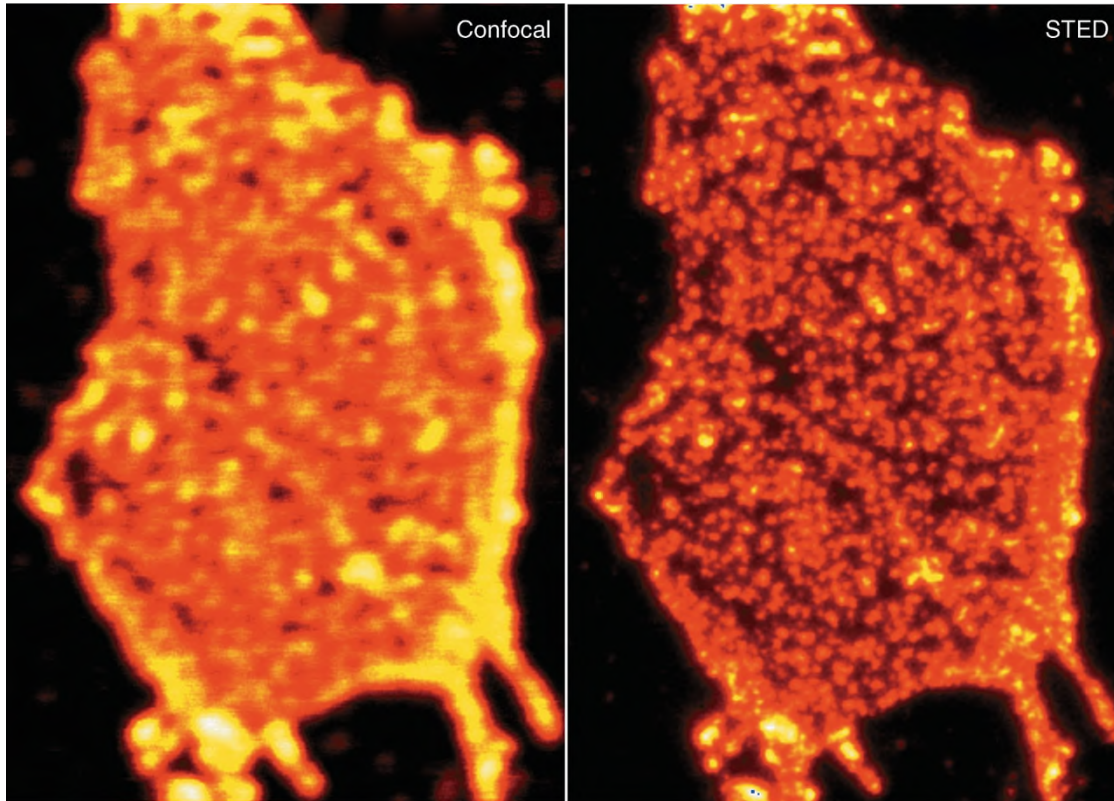


FIGURE 31.6. Resolution comparison of confocal versus STED-microscopy; plasma membrane patches immuno-stained against the SNARE protein SNAP25; secondary antibody labeled with Atto 532-NHS; Emission 540–570 nm, STED at 615 nm. The confocal image was recorded by simply turning off the STED beam with no other changes.

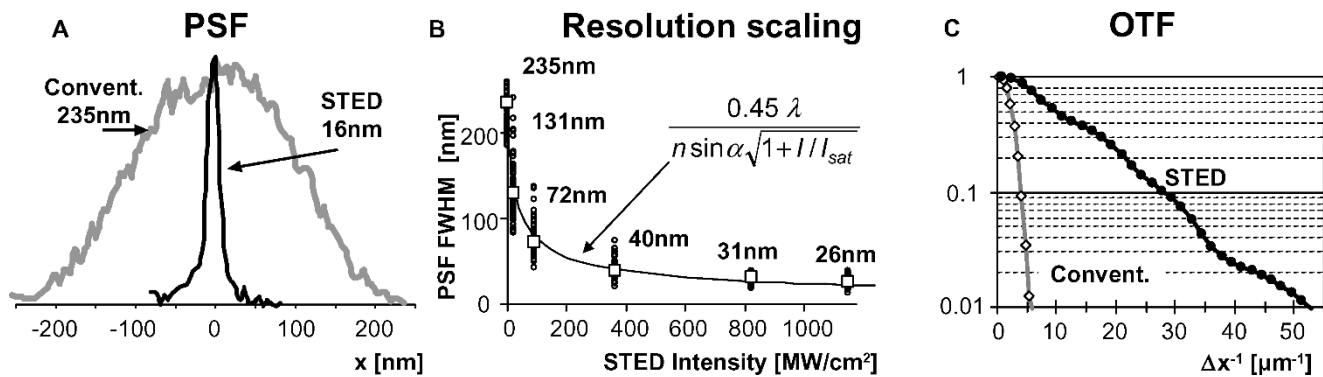


FIGURE 31.7. STED-microscopy hits the nanoscale. (A) Comparison of the PSF (x -axis) of a conventional and a STED microscope probed with a single dye molecule whose orientation is parallel to the polarization of the STED-beam; for details see (Westphal and Hell, 2005). The up-to 15-fold reduction in lateral width underscores the potential of STED-microscopy to attain true nanoscale resolution. (B) The resolution of a STED microscope scales with the square root of the intensity used in the STED beam, with no firm limit, as predicted by equation (4). The gain in resolution also entails an increase of the OTF bandwidth over the diffraction barrier. (C) Shows an example where the usable bandwidth (magnitude $>1\%$) of the OTF is broader by about an order of magnitude than in a conventional microscope. All measurements were performed with the red emitting dye JA26 and with a STED-wavelength of ~ 780 nm. Being a far-field optical microscope, the resolution of STED-microscopy increases inversely with the wavelength. Therefore, in (A) reducing the wavelength for STED to 500 nm would decrease the FWHM down to ~ 10 nm.

REFERENCES

- Abbe, E., 1873, Beiträge zur Theorie des Mikroskops und der mikroskopischen Wahrnehmung, *Arch. f. Mikroskop. Anat.* 9:413–420.
- Alivisatos, A.P., 1996, Semiconductor clusters, nanocrystals, and quantum dots, *Science* 271:933–937.
- Bruchez, M. Jr., Moronne, M., Gin, P., Weiss, S., and Alivisatos, A.P., 1998, Semiconductor nanocrystals as fluorescent biological labels, *Science* 281:2013–2015.
- Chudakov, D.M., Belousov, V.V., Zaraisky, A.G., Novoselov, V.V., Staroverov, D.B., Zorov, D.B., Lukyanov, S., and Lukyanov, K.A., 2003, Kindling fluorescent proteins for precise *in vivo* photolabeling, *Nat. Biotechnol.* 21:191–194.
- Cragg, G.E., and So, P.T.C., 2000, Lateral resolution enhancement with standing wave evanescent waves, *Opt. Lett.* 25:46–48.
- Dyba, M., and Hell, S.W., 2002, Focal spots of size $\lambda/23$ open up far-field fluorescence microscopy at 33 nm axial resolution, *Phys. Rev. Lett.* 88:163901.
- Dyba, M., and Hell, S.W., 2003, Photostability of a fluorescent marker under pulsed excited-state depletion through stimulated emission, *Appl. Opt.* 42:5123–5129.
- Dyba, M., Jakobs, S., and Hell, S.W., 2003, Immunofluorescence stimulated emission depletion microscopy, *Nat. Biotechnol.* 21:1303–1304.
- Eigen, M., and Rigler, R., 1994, Sorting single molecules: applications to diagnostics and evolutionary biotechnology, *Proc. Natl. Acad. Sci. USA* 91:5740–5747.
- Hänninen, P.E., Lehtelä, L., and Hell, S.W., 1996, Two- and multiphoton excitation of conjugate dyes with continuous wave lasers, *Opt. Commun.* 130:29–33.
- Heintzmann, R., and Cremer, C., 1998, Laterally modulated excitation microscopy: Improvement of resolution by using a diffraction grating, *SPIE Proc.* 3568:185–195.
- Heintzmann, R., Jovin, T.M., and Cremer, C., 2002, Saturated patterned excitation microscopy – A concept for optical resolution improvement, *J. Opt. Soc. Am. A* 19:1599–1609.
- Hell, S.W., 1997, Increasing the resolution of far-field fluorescence light microscopy by point-spread-function engineering, In: *Topics in Fluorescence Spectroscopy* (J.R. Lakowicz, ed.), Vol. 5, Plenum Press, New York, pp. 361–422.
- Hell, S.W., 2003, Toward fluorescence nanoscopy, *Nat. Biotechnol.* 21:1347–1355.
- Hell, S.W., 2004, Strategy for far-field optical imaging and writing without diffraction limit, *Phys. Lett. A* 326:140–145.
- Hell, S.W., and Kroug, M., 1995, Ground-state depletion fluorescence microscopy, a concept for breaking the diffraction resolution limit, *Appl. Phys. B* 60:495–497.
- Hell, S.W., and Wichmann, J., 1994, Breaking the diffraction resolution limit by stimulated emission: Stimulated emission depletion microscopy, *Opt. Lett.* 19:780–782.
- Hell, S.W., Jakobs, S., and Kastrup, L., 2003, Imaging and writing at the nanoscale with focused visible light through saturable optical transitions, *Appl. Phys. A* 77:859–860.
- Kastrup, L., Blom, H., Eggeling, C., and Hell, S.W., 2005, Fluorescence fluctuation spectroscopy in subdiffraction focal volumes, *Phys. Rev. Lett.* 94:178104.
- Klar, T.A., Engel, E., and Hell, S.W., 2001, Breaking Abbe's diffraction resolution limit in fluorescence microscopy with stimulated emission depletion beams of various shapes, *Phys. Rev. E* 64:1–9.
- Klar, T.A., Jakobs, S., Dyba, M., Egnér, A., and Hell, S.W., 2000, Fluorescence microscopy with diffraction resolution limit broken by stimulated emission, *Proc. Natl. Acad. Sci. USA* 97:8206–8210.
- König, K., Tadir, Y., Patrizio, P., Berns, M.W., and Tromberg, B.J., 1996, Effects of ultraviolet exposure and near-infrared laser tweezers on human spermatozoa, *Hum. Reprod.* 11:2162–2164.
- Levene, M.J., Korlach, J., Turner, S.W., Foquet, M., Craighead, H.G., and Webb, W.W., 2003, Zero-mode waveguides for single-molecule analysis at high concentrations, *Science* 299:682–686.
- Lukyanov, K.A., Fradkov, A.F., Gurskaya, N.G., Matz, M.V., Labas, Y.A., Savitsky, A.P., Markelov, M.L., Zaraisky, A.G., Zhao, X., Fang, Y., Tan, W., and Lukyanov, S.A., 2000, Natural animal coloration can be determined by a nonfluorescent green fluorescent protein homolog, *J. Biol. Chem.* 275:25879–25882.
- Magde, D., Elson, E.L., and Webb, W.W., 1972, Thermodynamic fluctuations in a reacting system – measurements by fluorescence correlation spectroscopy, *Phys. Rev. Lett.* 29:705–708.
- Peng, X., Manna, L., Yang, W., Wickham, J., Scher, E., Kadavanich, A., and Alivisatos, A.P., 2000, Shape control of CdSe nanocrystals, *Nature* 404:59–61.
- Schönle, A., Hänninen, P.E., and Hell, S.W., 1999, Nonlinear fluorescence through intermolecular energy transfer and resolution increase in fluorescence microscopy, *Ann. Phys. (Leipzig)* 8:115–133.
- Schönle, A., and Hell, S.W., 1999, Far-field fluorescence microscopy with repetitive excitation, *Eur. Phys. J. D* 6:283–290.
- Westphal, V., and Hell, S.W., 2005, Nanoscale resolution in the focal plane of an optical microscope, *Phys. Rev. Lett.* 94:143903.
- Westphal, V., Blanca, C.M., Dyba, M., Kastrup, L., and Hell, S.W., 2003, Laser-diode-stimulated emission depletion microscopy, *Appl. Phys. Lett.* 82:3125–3127.
- Westphal, V., Kastrup, L., and Hell, S.W., 2003, Lateral resolution of 28 nm ($\lambda/25$) in far-field fluorescence microscopy, *Appl. Phys. B* 77:377–380.